

Review

On the Importance of Electron Beam Brightness in High Gain Free Electron Lasers

Simone Di Mitri

Elettra–Sincrotrone Trieste S.C.p.A., S.S. 14 km 163,5 in Area Science Park, 34149 Basovizza, Trieste, Italy; E-Mail: simone.dimitri@elettra.eu; Tel.: +39-040-375-8778

Received: 4 March 2015 / Accepted: 24 March 2015 / Published: 27 March 2015

Abstract: Linear accelerators delivering high brightness electron beams are essential for driving short wavelength, high gain free-electron lasers (FELs). The FEL radiation output efficiency is often parametrized through the power gain length that relates FEL performance to electron beam quality at the undulator. In this review article we illustrate some approaches to the preliminary design of FEL linac-drivers, and analyze the relationship between the output FEL wavelength, exponential gain length and electron beam brightness. We extend the discussion to include FEL three-dimensional effects and electron beam projected emittances. Although mostly concentrating on FELs based upon self-amplified spontaneous emission (SASE), our findings are in some cases highly relevant to externally seeded FELs.

Keywords: free electron laser; gain length; electron beam brightness

1. Introduction

The physics of Free Electron Lasers (FELs) dates back to the 1970s [1–3] and is extensively treated in several recent textbooks (see for example [4–6]) and reviews [7–9], and supported by experimental results at several FEL facilities around the world that have exhibited lasing at wavelengths from the ultra-violet (UV) to hard X-rays [10–16]. The success achieved by FEL facilities in the light source user community in the last ~10 years is confirmed, also, by the inclusion of a Session devoted to “FEL Applications” in many editions of the International Free Electron Laser Conference. Such interchanges allow the accelerator and FEL community to stay in touch with the most advanced experimental techniques and results based on FEL sources. Similarly, the user community is exposed to advances in FEL physics and experimental methods that might open new frontiers in scientific research. Thus, it is

not surprising that a journal such as *Photonics* by MDPI would include technical works by both the accelerator and FEL scientific community. This review article recalls in a ready-to-use form various merit functions of high gain Self-Amplified Spontaneous Emission (SASE) FELs [17–20], in the one-dimensional (1-D) monochromatic electron beam approximation. Hereafter, “high gain” refers to the electron beam-radiation collective instability that results in an exponential growth of laser intensity [18,20–24]. The definition and the physical meaning of FEL merit functions forms the content of Section 2. These functions are used in Section 3 to illustrate three different approaches to the preliminary design of an FEL linac-driver. In Section 4, the electron beam parameters are condensed in one invariant of linear particle dynamics, the six-dimensional energy-normalized electron beam brightness. This brightness is shown to be highly correlated with the minimum obtainable wavelength of efficient FEL emission. Section 5 elaborates the relationship between electron beam brightness and so-called 3-D FEL effects. Since at this point the discussion had been limited to local properties (longitudinal “slice” parameters) of the electron bunch, the physics of FEL drivers is further extended to the characteristics of the electron beam as a whole, namely, to longitudinally “projected” parameters. Guidelines for the optimization of the newly defined “3-D, z-projected” electron beam brightness and FEL power gain length are reviewed in Section 6. We end by summarizing our conclusions in Section 7.

2. Merit Functions of High Gain Free Electron Lasers

The amplification of coherent SASE FEL intensity along the undulator is initiated by incoherent undulator emission. Lasing at the FEL fundamental wavelength has its maximum intensity at the same undulator on-axis central spontaneous emission wavelength:

$$\lambda = \frac{\lambda_u}{2\gamma^2} (1 + a_w^2) \tag{1}$$

Here γ is the relativistic Lorentz factor for the electron beam mean energy, λ_u the undulator period length, $a_w = K$ for helically- and $a_w = K/\sqrt{2}$ for planar-polarized undulator, where $K \equiv eB_0\lambda_u/(2\pi m_e c) = 0.934B_0[T]\lambda_u[cm]$ in practical units, is the so-called undulator parameter, B_0 the undulator peak magnetic field, and e and m_e the electron charge and rest mass, respectively, and c the speed of light in vacuum. K is linearly proportional to the electron’s amplitude of transverse oscillation in the undulator field and is typically in the range 1–5 for reasonable gain. Equation (1) is often referred to as the FEL “resonance condition” since it selects, for any undulator period and magnetic field strength, the necessary electron beam mean energy E for lasing at λ .

In the so-called 1-D, cold limit, where electron beam energy spread, transverse emittance and radiation diffraction effects are all neglected, the radiation peak power at the resonant wavelength grows exponentially along the undulator with a gain length $L_G = \lambda_u/(4\pi\sqrt{3}\rho)$. Here ρ is the “FEL parameter” [20] and is intimately related to the Pierce parameter relevant to the physics of microwave tubes [25]:

$$\rho = \left(\frac{\Omega_p \lambda_u a_w [JJ]}{8\pi c \gamma} \right)^{2/3} = \frac{1}{2\gamma} \left(\frac{I}{I_A} \right)^{1/3} \left(\frac{\lambda_u a_w [JJ]}{2\pi \sigma_x} \right)^{2/3} \tag{2}$$

with Ω_p being the plasma frequency, I the electron bunch peak current, $I_A = 17045$ A the Alfvén current, σ_x the standard deviation of the (assumed round) electron beam transverse size; a_w was defined in

Equation (1) and $[JJ]$ is the undulator-radiation coupling factor [26], equal to 1 for a helical undulator, and to $[J_0(\xi) - J_1(\xi)]$ for a planar undulator where J_0 and J_1 are Bessel's functions of the first kind with argument $\xi = K^2/(4 + 2K^2)$. Typically $\rho \approx 10^{-3}$ in the UV wavelength regime but may drop to $\sim 10^{-4}$ in the X-ray regime for kA-current beams. If the undulator length $N_u \lambda_u$, with N_u being the number of undulator periods, is equal or longer than $\sim 20 L_G$, the conversion of electrons' kinetic energy to photon energy considerably enlarges the electron beam energy spread, with an eventual reduction in the FEL gain; the associated FEL power saturates at a level $P_{\text{sat}} \approx 1.6\rho EI/e$. In spite of the low FEL extraction efficiency relative to the electron beam power (because $\rho \ll 1$), an electron beam at multi-GeV energies and kA-scale peak currents is able to produce GW-scale radiation peak powers. For SASE devices, the value of ρ also defines the approximate number of undulator periods $N_{\text{sat}} \sim 1/\rho$ and the length $L_{\text{sat}} \approx \lambda_u/\rho$ necessary to reach saturation. The normalized spectral bandwidth at saturation is $\Delta\omega/\omega \sim \rho$ presuming a more or less monoenergetic electron beam with little z-correlated energy spread.

The longitudinal evolution of the fine structure of the SASE FEL spectrum is determined by the longitudinal slippage of the radiation over the electrons, since the FEL resonance condition in Equation (1) requires that the radiation move ahead by one resonant wavelength per undulator period. This condition ensures a synchronized energy exchange between electrons and photons. The electrons' energy modulation is then transformed into density modulation ("micro-bunching") by the intrinsic energy dispersion associated to the wiggling motion in the undulator, and by the possible addition of dedicated magnetic insertions interleaving the undulator segments. The total slippage at the end of the undulator line is $s_L = N_u \lambda$ and usually $\leq 1 \mu\text{m}$ for hard X-rays, $\leq 10 \mu\text{m}$ for extreme-UV and soft X-rays, and larger than tens of μm at UV wavelengths. An optimum longitudinal overlap of electrons and photons requires that the total undulator slippage length be shorter than the electron bunch length. The slippage accumulated per one radiation gain length, $L_C = \sqrt{3}L_G(\lambda/\lambda_u) = \lambda/(4\pi\rho)$, is often called the "cooperation length" [27]: it is the longitudinal distance over which radiation coherence is preserved. A high gain SASE FEL output pulse consists of a number of power spikes in both the temporal and frequency regime approximately equal to the number of cooperation lengths contained in the electron bunch length. Near saturation, each individual spike has reasonably high coherence but there is essentially no coherence from spike to spike. Consequently, a SASE FEL radiation *pulse* is not Fourier transform limited, except when the electron bunch length is shorter than the cooperation length (in which case the extracted power efficiency is significantly smaller than the long bunch case).

Equation (2) applies to a monochromatic electron beam of non-zero transverse size, perfectly superimposed on the photon beam along the entire undulator. Realistic electron beams, however, have non-zero transverse emittances and energy spread, and the emitted radiation is affected by diffraction. Not surprisingly, all these effects act so as to reduce the effective ρ and thus the FEL performance from the hypothetical 1-D limit. Equation (1) suggests that the amplification rate of the FEL signal (gain) decreases as the energy spread of electrons distributed over one cooperation length increases. Once the spread in the longitudinal velocities of the electrons becomes sufficiently large to cause significant de-bunching over one power gain length, the FEL gain process strongly diminishes. Consequently, the

FEL gain grows exponentially as far as the following numerical condition applies to the beam fractional energy spread [28]:

$$\sigma_{\delta} \leq 0.5\rho \tag{3}$$

This spread in longitudinal velocities has two major sources: (1) the incoherent energy spread that is “uncorrelated” with the particle longitudinal position inside the bunch, and (2) the non-zero transverse emittance. The incoherent energy spread is typically in the range 0.1 to several MeV at the undulator, depending upon the manipulation of the electron energy distribution at low energy and the bunch length compression strength applied in the upstream accelerator to reach the target peak current. At this point, it is convenient to introduce some of the jargon used in electron beam dynamics. If an energy-to-longitudinal position correlation along the bunch is established before lasing—henceforth named “energy chirp”—as needed for magnetic compression and/or caused by longitudinal wakefields, σ_{δ} adds to the correlated energy spread and the resulting quantity, evaluated over a user-defined fraction of the bunch duration, is called “slice” energy spread. It is worth noticing that, in the presence of energy chirp, Equation (3) applies to the energy spread defined over a cooperation length or, with a stronger constraint, over the undulator slippage length. Energy spread and transverse emittances integrated over the entire bunch length are called “projected”, as opposite to their “slice” (local) counterparts. Equation (3) also holds as a rule-of-thumb for externally seeded FELs. For such devices, it additionally implies that for a given seed laser wavelength and undulator parameter, the electron beam mean energy should not deviate from its nominal resonant value by more than a fractional difference $\rho/2$ (more exactly, larger deviations lead to the local resonant wavelength falling out of the nominal FEL gain bandwidth).

Equation (3) refers both to the true energy spread and to the *effective* energy spread associated with the square of beam transverse angular divergence [29]. Beam divergence scales as $(\varepsilon/\beta_u)^{1/2}$, with β_u the average betatron function along the undulator and ε the geometrical electron beam transverse emittance (the two parameters are measured in the same plane; the divergences in the two planes add in quadrature). At the same time, in order to minimize emittance effects and to ensure optimal transverse overlap of the co-propagating radiation and electron beam, the electron beam trajectory, transverse size and angular divergence must be controlled with steering and quadrupole magnets that are interleaved between the undulator segments (similarly, the individual undulator magnet pole strengths and overall magnetic centerline tilt must also be carefully controlled but we will not discuss those issues here). The most efficient electron-photon beam interaction occurs when the transverse beam phase space area and distribution matches that of the radiation, whereas the transverse electron beam size scales as $(\varepsilon\beta_u)^{1/2}$. Considerations of both the maximum allowable effective energy spread and the transverse overlap lead to an rms value of ε that must be smaller than, or of the same order as, that of the diffraction-limited photon beam [30]:

$$\varepsilon \leq \frac{\lambda}{4\pi} \tag{4}$$

in order to maximize the FEL gain; this emittance value limit also optimizes the FEL transverse coherence. The aforementioned opposing scaling laws with β_u , instead, suggest that there is some optimal value of β_u (for any given ε and λ) that maximizes the FEL gain. At longer wavelengths, where diffraction effects can be important, one must also keep the effective Rayleigh range associated with the

electron beam area, which scales as $(\varepsilon\beta_u)/\lambda$, comparable to or greater than L_G . This diffraction constraint sets another lower limit to the value of β_u , apart from technological or transport limits.

As is well known, the horizontal (vertical) emittance is the area occupied by the particle ensemble in the x, x' (y, y') phase space, which is roughly the product of the transverse beam size and the transverse angular divergence. According to Liouville's theorem, its energy-normalized value is a constant of motion during acceleration in absence of dissipative forces and cross-dimensional coupling effects such as transverse/longitudinal emittance coupling or exchange schemes not covered by this review. In practice, the lower limit for the transverse emittance is set at the injector exit, beyond which the space charge forces become quite small and no longer act to rearrange the particles in phase space [31].

As was pointed out in [32], the three aforementioned conditions on energy spread, transverse emittance and diffraction length plus the resonance condition are not independent. At longer wavelengths (*i.e.*, $\lambda > 100$ nm), one may find that due to important diffraction effects, there comes a point where there are diminishing returns from decreasing the transverse emittance and optimizing β_u as compared with increasing the peak current. In the hard X-ray regime, where the electron beam energies are higher, technologically it might not be possible to decrease β_u below a certain value. In this case, however, radiation diffraction effects are much less important and the combination of lower emittance and higher peak current usually gives better FEL performance.

3. Approaches to FEL Linac-Driver Design

3.1. Pulse Length-Driven Approach

Strategies to design an FEL linac-driver strongly depend on the emphasis of the light source characteristics (intensity *vs.* bandwidth *vs.* wavelength tuning, *etc.*), and on the available or cost-allowable infrastructure (undulator length, linac length, *etc.*). Among many parameters, the FEL pulse duration is often the critical factor determining the electron beam parameters at the undulator and, to some extent, at the electron source.

The FEL pulse duration is typically specified by users in facilities relying on SASE, whilst its lower-limit is set by the duration of the external seed laser, such as in High Gain Harmonic Generation (HG) schemes [10,15,16,33–37]. In both cases, the electron bunch duration at the undulator should be longer than the required FEL pulse duration because of effects such as FEL slippage in SASE FELs, arrival time jitter, and multi-stage cascade in HG FELs. As an example in the soft X-rays, a 100 fs SASE FEL pulse duration (full width) may require a ≥ 150 fs electron bunch duration at the undulator.

Then, in a second step, we must specify the minimum FEL power at the shortest fundamental wavelength we want to reach and/or we are able to detect. A wavelength of, say 1 nm, allows us to estimate the required undulator parameter and the beam energy through the resonance condition in Equation (1): we come out with $K \sim 1$, $\lambda_u \sim 2.5$ cm and $\gamma \sim 5000$. Wavelength and beam energy also determine the upper value of the allowable beam normalized transverse emittance as in Equation (4), *i.e.*, $0.4 \mu\text{m rad}$. The minimum required FEL peak power at saturation, *e.g.*, 1 GW, provides the minimum peak current after total compression. ρ has not been defined yet, but we may guess a value around 10^{-3} for it, in the soft X-rays; thus we require $I [\text{A}] = P_{\text{sat}}[\text{GW}]/(1.6\rho E[\text{GeV}]) \geq 1.25$ kA. It is worth noting

that typically $\rho \approx 10^{-3}$ – 10^{-4} in the XUV wavelength range, which implies a peak current usually higher than 100 A at the undulator.

In a third step, peak current times electron bunch duration gives the minimum required bunch charge, $Q \sim 0.2$ nC. Bunch charge and normalized emittance help in turn to estimate the electron bunch duration at the injector (typically the higher the line charge density, the higher the transverse emittance) and, as a consequence, the total bunch length compression factor to reach the aforementioned peak current. From the practical point of view, several picosecond-long bunches generated by photo-injectors show a normalized emittance (in $\mu\text{m rad}$) proportional to the square or the cubic root of the total charge (in nC) [38]. A standard photo-injector design can therefore provide a bunch not shorter than ~ 5 ps FWHM for $Q = 0.2$ pC. The initial peak current turns out to be of the order of 40 A, and the total compression factor should be equal or larger than 30 to reach ~ 1.2 kA at the undulator.

A fourth step includes the estimation of the allowable uncorrelated energy spread at the injector (again, the higher the line charge density, the higher the energy spread). Its *final* value has to be compared to the FEL parameter in Equation (3). Since the final energy spread is linearly proportional to the compression factor, it sets an upper limit to the final peak current. This picture is actually complicated in practice by the artificial increase of energy spread before compression by means of a “laser heater” [39–41]. This device helps to minimize the microbunching instability that would otherwise strongly grow along the acceleration and compression stages, at the expense of FEL performance. The energy spread induced by a laser heater may be of the order of few tens of keV rms, typically dominating the few keV rms “natural” energy spread of the beam at the injector exit [42]. The final beam energy spread (uncorrelated) might therefore be close to, or smaller than, 1 MeV in our example; it will be larger in multi-GeV machines. That value fits well with $\rho \approx 1 \times 10^{-3}$ (Equation (2) for $\beta_u = 7$ m). We finally get $L_G = 1.1$ m, and the saturation length is 17 m. This kind of design strategy inevitably needs several iterations for convergence to a satisfactory and self-consistent set of the accelerator and electron beam parameters. Alternative approaches are discussed in the following two subsections.

3.2. Wavelength-Driven Approach (with Some Wavelength Tuning)

The fundamental wavelength of FEL emission and its tuning range is in most cases one of the earliest design parameters put on the table by the potential users. Not unlike the previous scenario, we assume $\lambda = 1$ nm with similar undulator characteristics, $K \sim 1$, $\lambda_u \sim 2.0$ cm. The resonance electron energy turns out to be around 2 GeV (Equation (1)). The beam energy could be higher if we require greater saturated FEL intensity, or if we chose a longer undulator period. Unlike in the previous discussion, these estimates will be subject to fine-tuning in the following steps.

An additional requirement from users is that, for example, of a range in FEL output wavelength, up to, say, $\lambda_{\text{max}} \sim 5$ nm. We decide that this tuning range will mainly be provided by adjustable gap undulators (alternatively, the beam energy could be varied). To this purpose, we adopt the hybrid permanent magnet undulator model that relates the peak magnetic field to the undulator period and the undulator gap, g [43]:

$$B_0 [T] = 4.22 \exp \left[-5.08 \times \frac{g}{\lambda_u} + 1.54 \times \left(\frac{g}{\lambda_u} \right)^2 \right], \text{ with } g \text{ in units of mm and}$$

λ_u in cm. The technological limit of a minimum gap, e.g., $g_{\text{min}} = 6$ mm, provides an upper limit to the achievable undulator field and, thus, of the undulator parameter, $K_{\text{max}} \approx 2$. These values of K_{max} and λ_{max}

provide a new estimate for the electron beam energy. If the undulator period is now also left free to be adjusted, the FEL resonance condition provides the equation $\gamma = \gamma(\lambda_u; \lambda_{\max}, K_{\max}(\lambda_u))$, by which the longer the period, the higher the required beam energy. This relationship is substituted in the resonance equation for $\lambda_{\min} = \lambda_{\min}(\lambda_u; \gamma(\lambda_u), K_{\min}) \equiv 1 \text{ nm}$; we also adopt a lower limit to K , e.g., 1.5, in order to prevent the gain length from becoming too large. From the condition $\lambda_{\min} = \lambda_{\min}(\lambda_u; \gamma(\lambda_u), K_{\min}) \equiv 1 \text{ nm}$ we obtain an undulator period around 2.8 cm, which corresponds in turn to the beam energy of 2.85 GeV. Going back in our reasoning, $K_{\max} = 4.5$ is required to ensure lasing at 4.8 nm, for an undulator gap of 6 mm.

By fixing the electron beam energy and the minimum lasing wavelength, we determine the highest allowable normalized emittance value, *i.e.*, 0.5 $\mu\text{m rad}$, which satisfies the mode overlap condition. A square root law with the charge (see above) suggests $Q = 0.25 \text{ pC}$ for, say, 8 ps FWHM long bunch at the injector. Since we have no specific requirements on the FEL output power, an initial guess of 1 kA bunch peak current, which is consistent with all other beam parameters in the previous subsection, is reasonable. The total compression factor then turns out to be ~ 30 and the final energy spread is likely of the order of 1 MeV. We are now able to compute 1-D parameters of lasing in SASE mode. At 1 nm we obtain $\rho = 0.9 \times 10^{-3}$, $L_G = 1.4 \text{ m}$, and a peak power at saturation of 3 GW over approximately 0.27 ps FWHM pulse duration.

3.3. Cost-Driven Approach

Another approach to the design of an FEL linac driver might be that of minimizing the size of infrastructures, linac and undulator length *in primis*, in order to be cost effective. Once again, we start with a target output radiation wavelength of 1 nm. Although the electron beam geometrical emittance and fractional energy spread are expected to improve with the beam energy, the “equivalent” undulator length needed to reach a certain wavelength gets longer as the beam energy increases. We therefore proceed in the opposite direction and choose the minimum beam energy that is compatible with the shortest feasible undulator period. Very short periods can be provided by in-vacuum undulators and can be as short as 15 mm, with $K \approx 1$, typically at the expense of a very small tuning range in K . Equation (1) is used to deduce a beam energy of 1.7 GeV (alternatively, we could have chosen, e.g., $K \approx 2$ to obtain a beam energy comparable to that estimated in the previous approaches, but with a much higher radiation flux). It is worth mentioning that other, more recent solutions for shortening the undulator period and therefore using electron bunches with much lower energy, could be considered for a more aggressive, cost-effective FEL design, such as microwave, superconducting, and optical undulators [44–47].

Staying for the moment with the in-vacuum undulator, Equation (4) tells us that the normalized emittance must be equal to, or smaller than, 0.3 $\mu\text{m rad}$. As an initial guess, we assume a bunch charge of 100 pC, and an initial bunch duration of 5 ps FWHM. The initial bunch peak current is therefore around 20 A. If we were able to have $\rho \approx 0.5 \times 10^{-3}$, then the peak current at the undulator to reach 1 GW of power at saturation would be higher than 740 A, and the needed compression factor larger than 35 (for a 0.14 ps long bunch). In this case, the final fractional rms energy spread should not exceed 0.5 MeV (Equation (3)). We now compute ρ as in Equation (2) and find that it is 0.8×10^{-3} for $\beta_u = 7 \text{ m}$, not far from our initial guess. In this case $L_G = 0.9 \text{ m}$, and the SASE saturation length is shorter than 20 m.

4. Six-Dimensional Electron Beam Brightness

4.1. Definition

The 6-D normalized electron beam brightness may be defined as the total bunch charge divided by the product of the rms horizontal, vertical and longitudinal normalized emittances. In general, we may define the brightness locally, *i.e.*, either for each bunch *slice* (in this case, the brightness depends on the *z*-coordinate inside the bunch) or for the entire bunch, thus involving the bunch total charge and *projected* emittances. The normalized longitudinal emittance scales as the product of bunch length and absolute energy spread. The transverse normalized emittances are invariant under acceleration and linear transport, presuming collective effects, such as space charge, may be neglected. The same is true for the longitudinal normalized emittance if the energy spread is uncorrelated, *i.e.*, without any chirp.

The presence of nonlinear motion and collective effects along the beam delivery system may dilute the normalized emittances from their values at the injection point. We introduce an effective degradation factor $\zeta \geq 1$ in each plane of the particle motion so that $\epsilon_{nx,f} = \zeta_x \gamma_0 \epsilon_{x,0}$, $\epsilon_{ny,f} = \zeta_y \gamma_0 \epsilon_{y,0}$ and $\epsilon_{nz,f} = \sigma_{z,f} \sigma_{E,f} = \zeta_z \sigma_{z,0} \sigma_{E,0}$ with obvious notation. We are now able to relate the 6-D normalized brightness at the undulator, $B_{n,f}$, to that at the linac injection, $B_{n,0}$ [48]:

$$B_{n,f} \equiv \frac{Q}{\epsilon_{nx,f} \epsilon_{ny,f} \epsilon_{nz,f}} = \frac{Q}{\zeta_x \zeta_y \zeta_z \gamma_0^2 \epsilon_{x,0} \epsilon_{y,0} \sigma_{z,0} \sigma_{E,0}} = \frac{B_{n,0}}{\zeta_x \zeta_y \zeta_z} \quad (5)$$

In the ideal case of vanishing nonlinear and collective effects, $\zeta_x, \zeta_y, \zeta_z \rightarrow 1$ in Equation (5), and thereby the 6-D normalized brightness is preserved at the injector level under acceleration and linear bunch length compression. We remark that even in the absence of emittance degradation, the normalized 5-D electron beam brightness given by $B_{n,f} \times \sigma_E$, is not invariant under compression: it is actually linearly proportional to the total bunch length compression factor.

4.2. Scaling Laws

The importance of electron beam brightness for FELs [49] is underlined by Equation (2) for ρ , which is defined in terms of electron beam energy, peak current and transverse beam size. Since a smaller transverse emittance is usually associated with shorter FEL wavelengths, and since we can observe a qualitative proportionality between transverse emittance and $B_{n,f}$, we wonder if we could establish any relationship between $B_{n,f}$, and λ . This is done below, neglecting for the moment any emittance dilution, by substituting Equation (1) and Equation (4) into Equation (5), and assuming the electron beam transverse emittance (equal in the two planes) equals the diffraction limit of Equation (4):

$$B_{n,f} \equiv \frac{Q}{\epsilon_{nx,f} \epsilon_{ny,f} \epsilon_{nz,f}} = \frac{I}{c \sigma_E \gamma_0^2 \epsilon_0^2} \approx \frac{32\pi^2}{c} \frac{I}{\sigma_E} \frac{1}{\lambda_u} \frac{1}{(1+a_w^2)} \frac{1}{\lambda} \quad (6)$$

It is worth noticing that the ratio I/σ_E is invariant under acceleration (whereas the peak current and the energy spread must be evaluated at the same location along the accelerator) and compression when collective effects are ignored, so that, for any given set of undulator characteristics, shorter λ require higher $B_{n,f}$. This is confirmed empirically in Figure 1, where $B_{n,f}$ of designed and existing single-pass

linac-driven FEL facilities, is shown as function of the maximum photon energy (*i.e.*, minimum fundamental wavelength) from UV to X-rays (inferred or measured data are taken from [49] and updated to 2013). Moreover, Figure 1 shows $B_{n,f}$ evaluated for projected and slice emittances (where the slice length is approximately one tenth of the total bunch duration, and located in the bunch core). A gap of one or two orders of magnitude occurs typically between the two brightness values. This is mainly due to the dilution of the transverse projected emittances and of the slice energy spread generated by correlations between different slice coordinates [48]. The closer the projected and the slice brightness, the more efficient the FEL process is going to be, since most of the electrons will be distributed in identical manner in 5-D (x, x', y, y', γ) phase space along the bunch. Usually, a smaller gap between the projected and the slice brightness is gained at the expense of the flexibility of the FEL facility in wavelength, intensity, polarization, *etc.* It is a remarkable achievement of the FEL community that the physics and computer model of these facilities have found an excellent confirmation in their operation over a relatively wide range of parameters.

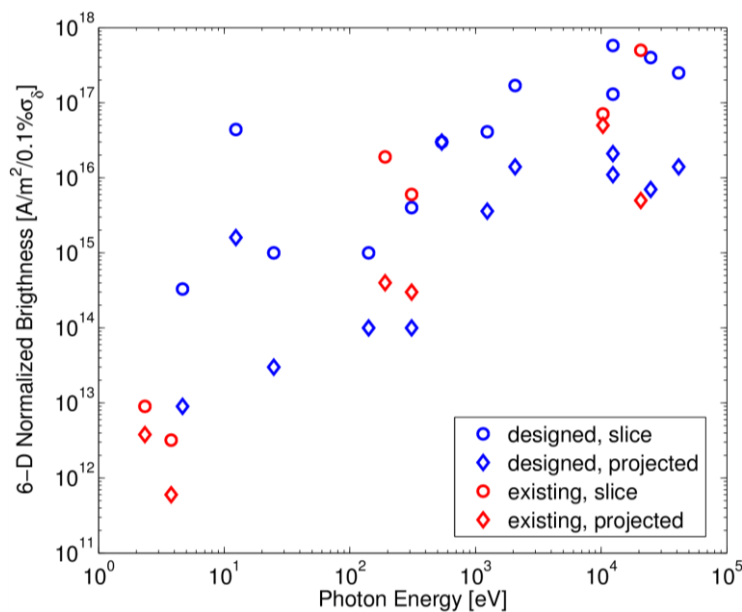


Figure 1. Six-dimensional normalized electron beam brightness vs. maximum photon energy at fundamental FEL emission, for facilities in the ultra-violet (UV) to X-rays, designed (blue) or running (red). Data taken from [49] and updated to 2013. From lower to higher energies, now-running facilities are: SPARC (Italy), SDUV-FEL (China), FLASH-I (Germany), FERMI (Italy), LCLS (USA), SACLA (Japan). The brightness refers to the projected (circle) or slice value in the bunch (diamond).

So as λ is a fundamental parameter for a given experiment, $\rho(\lambda)$ determines the efficiency of the electron-to-photon energy transfer in the undulator at that wavelength. In general, a large ρ is desired at any λ because this implies a shorter gain length, or a higher FEL power at saturation. Some restrictions to the upper value of ρ may be considered in a SASE FEL that targets a relatively narrow spectral bandwidth because in this kind of FEL, the output bandwidth is also proportional to ρ . We can explicit the dependence of ρ on $B_{n,f}$ by substituting Equation (6) into Equation (2), similarly to what was done in [50]

for the longitudinal brightness. We impose $4\pi\varepsilon = \lambda$, re-define the energy spread in Equation (6) like the rms value of γ , and consider a specific, typical value $K = 1$ in a helical undulator. Finally we get:

$$\rho \approx 0.016 \frac{E[\text{GeV}]^{4/3} \lambda[\text{nm}]}{\beta_u[m]^{1/3}} \sigma_\delta^{1/3} B_{n,f} \left[\frac{A}{\mu\text{m}^2} \right]^{1/3}, \quad (7)$$

from which we see that the strongest dependence of ρ is on the electron beam energy. The latter is easy to be increased with a longer linac or higher accelerating gradient RF structures, but it is also quite expensive. It is worth noting that since the FEL resonance condition in Equation (1) imposes $\lambda \sim 1/E^2$, ρ is not expected to vary much when λ is made short, and in fact we typically have $\rho \approx 10^{-3}$ – 10^{-4} in the entire XUV range (*i.e.*, $\lambda \approx 0.1$ – 100 nm). Equation (7) can be further manipulated and ρ written as a function of the electron beam transverse and longitudinal parameters at the undulator, whereas still we retain $4\pi\varepsilon = \lambda$ and $K = 1$:

$$\rho \approx 3.1 \times 10^{-4} \left(\frac{I[A] \varepsilon_{n,x}[\mu\text{m}]}{\beta_u[m]} \right)^{1/3} \quad (8)$$

Equation (8) tells us that, in order to have ρ large at any given λ , it is always convenient to increase the peak current, while there is no practical convenience in reducing the emittance below the diffraction limit, because this would reduce ρ with much improvement neither in the FEL output power, nor in the FEL transverse coherence.

5. Gain Length and Electron Beam Slice Parameters

5.1. Three-Dimensional Gain Length

The optimization of an FEL design usually involves minimization of the FEL power gain length [20,32]. For many years, FEL theories that include 3-D effects have been proposed [51,52] to predict the gain length and other FEL parameters when the 1-D approximation falls short of a realistic physics model. In recent times, two analytical models [53–55] have been commonly used to estimate the so-called 3-D gain length, $L_{G,3D}$ that takes into account the electron beam non-zero transverse emittance, energy spread and radiation diffraction in SASE FELs. For the sake of brevity, in the remainder of this article we will neglect the detuning parameter [53]. In those models, the emittance and the energy spread are those of a longitudinal slice of the electron bunch. The slice length is assumed to be of the order of the FEL cooperation length, thus typically much shorter than the total bunch duration. An additional 3-D effect involving the projected electron distributions, which is the impact of transverse deviations of the electron bunch’s trajectory from its reference path in the undulator on L_G , was modeled in [56] and experimentally studied in [57]. This Section will treat the FEL slice dynamics only; the projected dynamics is postponed to the next Section.

For a given set of electron beam and undulator parameters, the analytical model for 3-D FEL effects given in [53] by M. Xie allows the minimization of $L_{G,3D}$ as function of the average betatron function in the undulator, presuming the electron beam is well-matched to the design optics. According to [53], the 3-D power gain length is:

$$L_{G,3D}^{MX} = L_G(1 + \Lambda); \tag{9}$$

$$\Lambda = a_1\eta_d^{a_2} + a_3\eta_\varepsilon^{a_4} + a_5\eta_\gamma^{a_6} + a_7\eta_\varepsilon^{a_8}\eta_\gamma^{a_9} + a_{10}\eta_d^{a_{11}}\eta_\gamma^{a_{12}} + a_{13}\eta_d^{a_{14}}\eta_\varepsilon^{a_{15}} + a_{16}\eta_d^{a_{17}}\eta_\varepsilon^{a_{18}}\eta_\gamma^{a_{19}}$$

with Λ a polynomial expression of three additional parameters, η_d , η_ε and η_γ , addressing, respectively, the effects of radiation diffraction, the electron beam transverse emittance and uncorrelated energy spread. For the Reader’s convenience, we report here also the 19 coefficients used in Equation (9): $a_1 = 0.45$, $a_2 = 0.57$, $a_3 = 0.55$, $a_4 = 1.6$, $a_5 = 3$, $a_6 = 2$, $a_7 = 0.35$, $a_8 = 2.9$, $a_9 = 2.4$, $a_{10} = 51$, $a_{11} = 0.95$, $a_{12} = 3$, $a_{13} = 5.4$, $a_{14} = 0.7$, $a_{15} = 1.9$, $a_{16} = 1140$, $a_{17} = 2.2$, $a_{18} = 2.9$, $a_{19} = 3.2$.

The *electric field* gain length defined by E. Saldin *et al.* in [54,55], instead, is the result of an analytical approach in which the undulator average betatron function has already been optimized to minimize it. It is worth noting that the equivalent *power* gain length is a factor 2 *smaller* than the expression given in [54] and thus it turns out to be:

$$L_{G,3D}^{ES} = L_{G,0}(1 + \chi), \text{ with :} \tag{10}$$

$$L_{G,0} \cong 0.8 \left(\frac{I_A}{I} \right)^{1/2} \frac{(\varepsilon_n \lambda_u)^{5/6}}{\lambda^{2/3}} \frac{(1 + K^2)^{1/3}}{K[JJ]}, \quad \chi = 131 \left(\frac{I_A}{I} \right)^{1/2} \frac{\varepsilon_n^{5/4}}{\lambda^{1/8} \lambda_u^{9/8}} \frac{\sigma_\delta^2}{(K[JJ])^2 (1 + K^2)^{1/8}}$$

Figures 2–4 show a remarkable agreement between the power gain length computed with the two models, as well as for the optimum betatron function, with a maximum discrepancy of 20%. The comparison relies on the baseline parameters in Table 1.

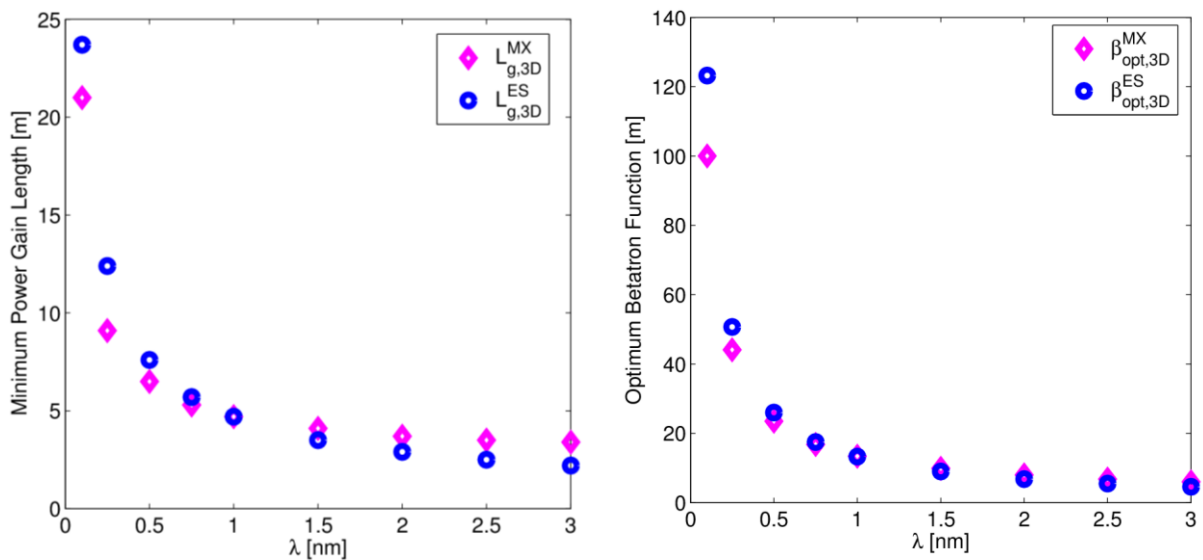


Figure 2. Minimum 3-D power gain length (**left**) and optimum betatron function (**right**) as function of the FEL fundamental wavelength, for the M. Xie (circles) and E. Saldin *et al.* (dots) formulas.

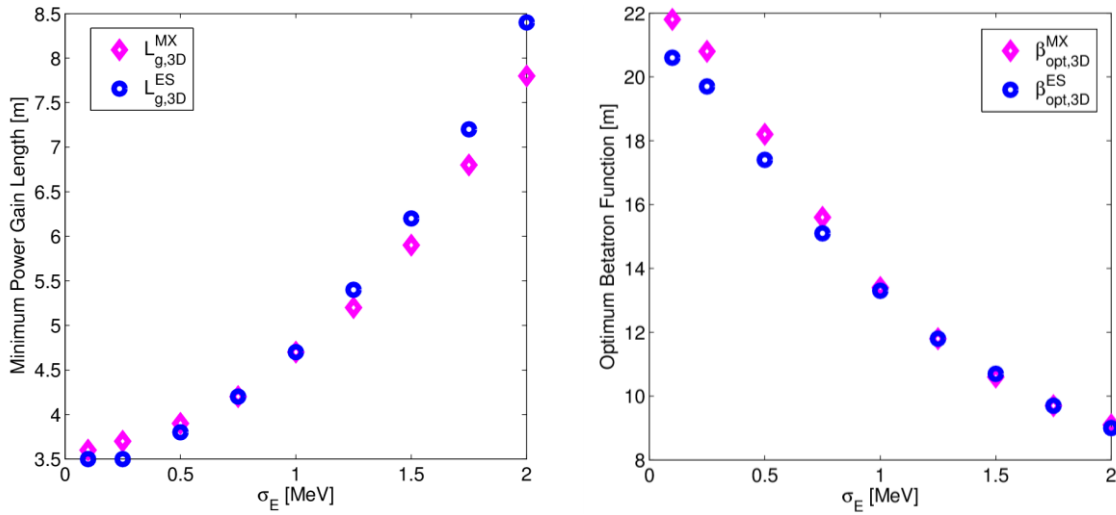


Figure 3. Minimum 3-D power gain length (left) and optimum betatron function (right) as function of the slice rms energy spread at the undulator, for the M. Xie (circles) and E. Saldin *et al.* (dots) formulas.

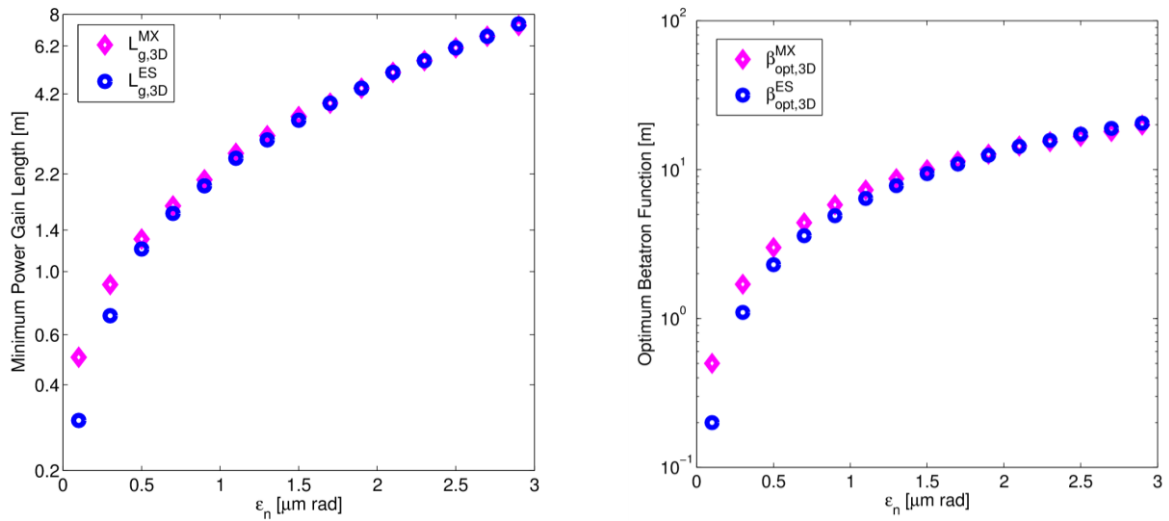


Figure 4. Minimum 3-D power gain length (left) and optimum betatron function (right) as function of the slice normalized transverse emittance at the undulator, for the M. Xie (circles) and E. Saldin *et al.* (dots) formulas.

Table 1. List of parameters for SASE FEL used to compare M. Xie [53] and E. Saldin *et al.* [54] 3-D power gain length.

Parameter	Value	Unit
Energy	2.8	GeV
Peak Current	2.5	kA
Norm. Trasn. Emittance, rms	2.0	$\mu\text{m rad}$
Energy Spread, rms	1.0	MeV
Undulator RMS Parameter, K	1	
Undulator Type	Planar	
Undulator Period Length	20	mm
Fundamental Wavelength	1.0	nm

5.2. Gain Length and Electron Beam Brightness

Given the substantial equivalence of the two aforementioned definitions of $L_{G,3D}$, in the following we will use that of M. Xie as it provides the additional degree of freedom on β_u . We will now analyze the dependence of L_G and $L_{G,3D}$ on the electron beam parameters, also taking advantage of the brightness definition in Equation (5). As for the 3-D case, an exact dependence of $L_{G,3D}$ on the brightness would lead to an excessively complicated expression with poor physical meaning. Instead, we prefer to look at the individual dependence of η_d , η_ϵ and η_γ on the electron beam parameters. Minimizing the three parameters translates into the minimization of Λ , thus of $L_{G,3D}$. Since L_G is just inversely proportional to ρ , we have from Equation (2):

$$L_G = \frac{1}{\sqrt{3}} \left(\frac{I_A}{2\pi} \right)^{1/3} \frac{(\lambda_u \beta_u)^{1/3}}{(a_w [JJ])^{2/3}} \gamma^{2/3} \left(\frac{I}{\epsilon_n} \right)^{-1/3} \tag{11}$$

The M. Xie 3-D perturbative terms previously introduced in Equation (9) turn out to be:

$$\begin{aligned} \eta_d &= \frac{\lambda \lambda_u}{4\pi \sqrt{3} \rho} \frac{1}{\sigma_x^2} = \frac{1}{2\sqrt{3}} \left(\frac{I_A}{2\pi} \right)^{1/3} \frac{(1+a_w^2)}{(a_w [JJ])^{2/3}} \lambda_u^{4/3} \frac{1}{\beta_u^{2/3}} \frac{1}{\gamma^{1/3}} (I \epsilon_n^2)^{-1/3}, \\ \eta_\epsilon &= \frac{\lambda_u}{\sqrt{3} \rho} \frac{\epsilon_n}{\beta_u \gamma \lambda} = \frac{4}{\sqrt{3}} \frac{I_A^{1/3}}{(1+a_w^2)} \left(\frac{2\pi}{\lambda_u a_w [JJ]} \right)^{2/3} \frac{1}{\beta_u^{2/3}} \gamma^{5/3} \left(\frac{I}{\epsilon_n^4} \right)^{-1/3}, \\ \eta_\gamma &= \frac{\sigma_\delta}{\sqrt{3} \rho} = \frac{2\sigma_\delta}{\sqrt{3}} I_A^{1/3} \left(\frac{2\pi}{\lambda_u a_w [JJ]} \right)^{2/3} \beta_u^{1/3} \gamma^{2/3} \left(\frac{I}{\epsilon_n} \right)^{-1/3} \end{aligned} \tag{12}$$

In Equation (12), we underline the dependence upon the “variables” peak current, emittance and γ (that relates to the resonance condition); all other symbols have been intended to be considered as fixed parameters. All 3-D terms are minimized by larger peak currents and smaller normalized (transverse) emittance, with the sole exception of the diffraction term that, instead, is minimized by a larger emittance. We show in Figure 5 the dependence of η_d , η_ϵ and η_γ on I and ϵ_n as given in Equation (12). In this case, current and emittance are treated as independent variables, which means that bunch charge and/or compression factor are not kept constant. All other parameters are defined in Table 1. Since diffraction is typically more important at longer wavelengths than at those in the X-ray regime, FELs lasing at wavelengths shorter than ~ 10 nm are mainly sensitive to η_ϵ and η_γ . That is, the FEL gain is larger for a lower normalized emittance and energy spread, and for a higher peak current electron beam. A compromise between these three parameters will, to a certain extent, optimize the gain at the shortest wavelengths.

Figure 5 does not take into account the impact of incoherent energy spread and, in a more general sense, the 6-D electron beam brightness upon the 3-D dynamics. First, we have to consider that, experimentally, peak current, normalized emittance and energy spread are inter-dependent. We have previously pointed out that the lower limit for the normalized emittance value is set at the injector exit, where it strongly depends on the bunch charge: $\epsilon_n \propto Q^\alpha$, where α was empirically found to be in the range $1/2-1/3$ (see for example [38]). At the same time, $I \propto Q$ through the compression factor, C . If the longitudinal emittance is approximately preserved, that is the product of bunch length and absolute uncorrelated energy spread is constant through the accelerator, then we also have $\sigma_\delta \propto \gamma \times I$. The latter

approximation typically holds when a laser heater is adopted to increase the uncorrelated energy spread of the beam at the injector’s exit in order to suppress the microbunching instability (see Section 3.1). It may also happen, however, that the larger the C to reach the desired I, the larger the laser heater-induced energy spread is in order to damp the microbunching instability. In practice, a trade-off can be found between the strength of magnetic compression (*i.e.*, peak current) and laser heater action (*i.e.*, energy spread). The interplay of transverse emittance, peak current, and energy spread on the 6-D brightness will be elucidated in the next section. For the moment, let us note that, according to Equation (5), $B_{n,f}$ is an invariant under acceleration, linear transport and compression, because it is the product of two invariants, ϵ_n and I/σ_E . The latter is the ratio of peak current and absolute energy spread evaluated at the same location along the accelerator. Let us suppose of fixing $\lambda = 1$ nm in our FEL design, $\gamma = 2$ GeV and $K \approx 1$. We may then start specifying $\epsilon_n \sim 1$ $\mu\text{m rad}$ with Equation (4), $\sigma_\delta \sim 0.1\%$ with Equation (3), and I larger than a few hundred Ampere, in order to have enough FEL intensity in a few gain lengths. A unique value for $B_{n,f}$ is therefore determined according to Equation (5). Looking at Figure 1, the value of $B_{n,f}$ is expected to be in the range 10^{16} – 10^{17} A/m²/0.1% σ_δ . We now wonder if it may be convenient, for a fixed target value of $B_{n,f}$, to design our FEL driver in order to (un)balance the invariant ϵ_n vs. the invariant I/σ_E . That is, lower peak current or larger energy spread can be accepted at the expense of smaller emittance, and *vice versa*. Figure 1 suggests that this makes sense if the variation of those parameters remains within the hyperspace defined by Equations (2), (3) and (4).

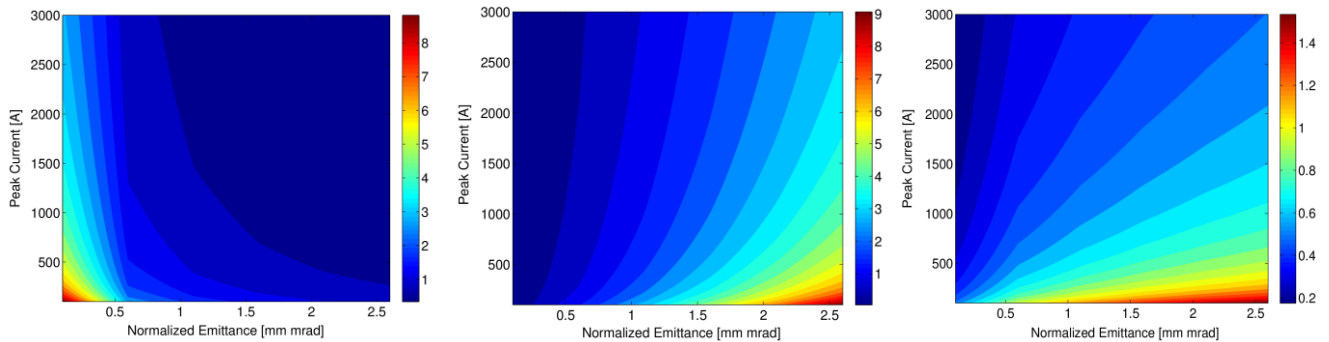


Figure 5. Contour plot of (from left to right) η_d , η_ϵ and η_γ as function of electron bunch peak current and rms normalized transverse emittance (see Equation (12)). All other beam and undulator parameters are listed in Table 1.

A quantitative guideline to such balance can be found below, where η_d , η_ϵ and η_γ are expressed as function of $B_{n,f}$; by doing so, we make evident their dependence on the emittance (the transverse invariant) and the fractional energy spread (which contains the information on the longitudinal invariant).

$$\begin{aligned}
 \eta_d &= \frac{\lambda \lambda_u}{4\pi\sqrt{3}\rho} \frac{1}{\sigma_x^2} = \frac{1}{2\sqrt{3}} \left(\frac{I_A}{2\pi} \right)^{1/3} \frac{(1+a_w^2)}{(a_w[J])^{2/3}} \lambda_u^{4/3} \frac{1}{\beta_u^{2/3}} \frac{1}{\gamma^{2/3}} \frac{1}{(cB_{n,f})^{1/3}} \frac{1}{\epsilon_n^{4/3} \sigma_\delta^{1/3}} \\
 \eta_\epsilon &= \frac{\lambda_u}{\sqrt{3}\rho} \frac{\epsilon_n}{\beta_u \gamma \lambda} = \frac{4}{\sqrt{3}} \frac{I_A^{1/3}}{(1+a_w^2)} \left(\frac{2\pi}{\lambda_u a_w [J]} \right)^{2/3} \frac{1}{\beta_u^{2/3}} \frac{\gamma^{4/3}}{(cB_{n,f})^{1/3}} \frac{\epsilon_n^{2/3}}{\sigma_\delta^{1/3}} \\
 \eta_\gamma &= \frac{\sigma_\delta}{\sqrt{3}\rho} = \frac{2\sigma_\delta}{\sqrt{3}} I_A^{1/3} \left(\frac{2\pi}{\lambda_u a_w [J]} \right)^{2/3} \beta_u^{1/3} \frac{\gamma^{1/3}}{(cB_{n,f})^{1/3}} \frac{\sigma_\delta^{2/3}}{\epsilon_n^{1/3}}
 \end{aligned} \tag{13}$$

Figure 6 shows η_d , η_ε and η_γ in the emittance and energy spread space, according to Equation (13). Now $B_{n,f}$ is kept fixed and therefore larger emittance or energy spread implies larger peak current. Not surprisingly, η_d and η_ε does not depend much on the energy spread, while they ask for opposite optimization of the emittance value. On the contrary, the right plot in Figure 6 for η_γ suggests there is some room for balancing emittance and energy spread. Last but not least, one should consider that a lower energy spread favors narrow bandwidth FEL emission in externally seeded FELs, and higher harmonic content of the electron bunching in both SASE and seeded FELs. This is an additional, fundamental consideration that brings to our attention the importance of $B_{n,f}$ for FEL performance (thus spectral properties in addition to intensity) instead of individual beam parameters, independently optimized.

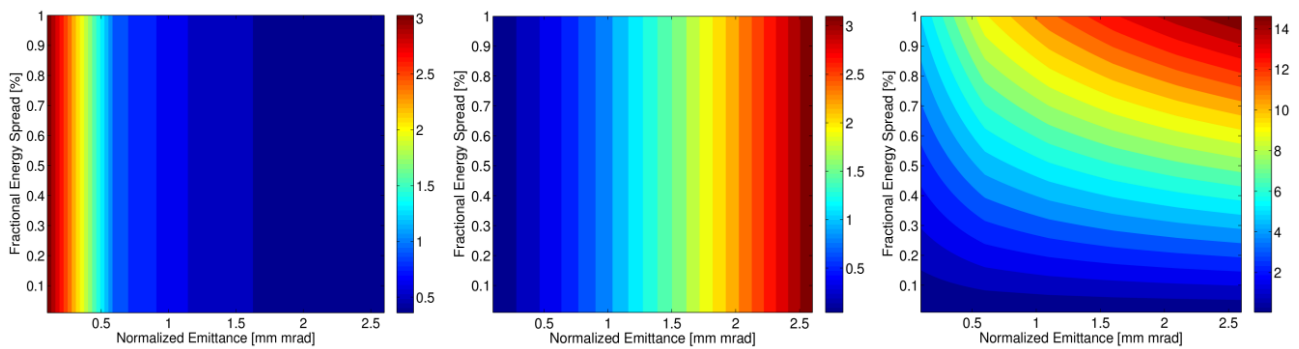


Figure 6. Contour plot of (from (left) to (right)) η_d , η_ε and η_γ as function of electron bunch fractional energy spread and normalized transverse emittance (all rms values, see Equation (13)). All other beam and undulator parameters are listed in Table 1.

6. Importance of Electron Beam Projected Emittance

6.1. Considerations for FEL Operation

The physical meaning of the cooperation length is that the FEL coherence develops locally over relatively short fractions of the electron bunch length. For realistic electron beams, the slice emittance and slice energy spread may vary significantly along the bunch and thus produce local regions where lasing may or may not occur. One could therefore argue that only *slice* electron beam quality is of interest, with each slice being as long as the FEL slippage length. In practice, however, other considerations related to the electron beam control and optimization of the FEL performance justify an optimization of both slice *and* projected beam emittances [49,58,59]. In the following, we extend the 3-D gain length theory to include the influence of the projected *transverse* emittance. For an inclusion of the projected longitudinal emittance the Reader is kindly referred to [48].

The need to control beam size and angular divergence along the undulator calls for measurements and the manipulation of the electron beam Twiss (envelope) parameters, which must be matched to the design Twiss parameters [60–62]. As a practical matter, optics matching is routinely performed experimentally by measuring the *projected* electron bunch transverse size [63]. From an operational point of view, it is therefore important to ensure that the projected transverse emittances and Twiss parameters be as close as possible to the slice ones, because this guarantees that most of the bunch slices are matched to the design optics and that they overlap in the transverse phase space. During beam

transport and acceleration, at least two collective effects threaten locally to offset bunch slices in the transverse (and longitudinal) phase space, namely coherent synchrotron radiation (CSR) and geometric transverse wakefields (GTW) (for a review of these topics, see for example [49]). Specific optics designs can be adopted to minimize these collective effects.

We also want to stress why the projected emittance can be considered a good marker for externally-seeded FEL performance. In HGHG FELs, the harmonic emission originates with a coherent electron energy modulation induced by an external laser, that interacts with the electron beam in a short, relatively longer period undulator (the “modulator”). Modulation at the seed laser wavelength provides, with the additional aid of a dedicated dispersive magnet, a microbunching rich in harmonic content. The electron beam finally radiates in a shorter period, longer undulator (the “radiator”). Output HGHG FEL properties reflect the high longitudinal coherence of the seeding laser, which can be tens to hundreds of femtoseconds long. In order to maximize the FEL parameter (Equation (2)) and the peak current, the final bunch duration is commonly specified to be only as long as the seed laser duration plus some room for accommodating the shot-to-shot arrival time jitter of the electron bunch with respect to the seed laser. Consequently, high performance from a seeded FEL requires uniformity of the slice beam parameters over most of the bunch duration in order to ensure the same strength of lasing from different slices. Thus, seeded FELs also require a large value of $B_{n,f}$, the brightness referred to *projected* transverse and longitudinal emittances.

6.2. 3-D Gain Length Including Projected Emittance

GTW and CSR perturb individual bunch “macro-slices” both in transverse configuration and velocity space. Neglecting for the moment any slice emittance growth from the injector to the undulator, the projected emittance growth is entirely due to mismatch of the bunch macro-slices in the transverse phase space. We take this growth into account through the mechanism described by Tanaka *et al.* [56]. In that work, the authors identify two distinct processes that increase LG. In the literature, the first effect is referred to as the (lack of) electron-photon transverse spatial overlap along the undulator. The second one describes the accumulation of longitudinal phase error between electrons and radiation by virtue of the slowing down of individual electrons due to their local angular divergence. We recognize that the electrons’ angular divergence has two contributions: one is incoherent and due to the non-zero beam emittance as depicted in Xie’s [53] and Saldin’s [54] models; the other is coherent, originating from the possible tilt of the macro-slice centroids with respect to the reference trajectory. The coherent divergence adds to (and in some cases, surpasses) the incoherent one and may amplify the effect of bunching smearing. One source of coherent divergence occurs when each macro-slice is transversely kicked by collective effects in the linac and can move along the undulator on a trajectory different from that of other macro-slices. If $\sqrt{\langle \theta_{coll}^2 \rangle}$ is the rms z-projected angular divergence of the macro-slice centroids at the undulator, and the charge transverse distribution at the undulator is matched to some design Twiss parameters, then the determinant of the so-called “sigma matrix” [64] computed at the undulator can provide the beam projected emittance as a function of $\sqrt{\langle \theta_{coll}^2 \rangle}$ and β_u :

$$\epsilon_{n,f} \approx \epsilon_{n,0} \sqrt{1 + \frac{\gamma \beta_u \langle \theta_{coll}^2 \rangle}{\epsilon_{n,0}}} \tag{14}$$

with $\epsilon_{n,0}$, $\epsilon_{n,f}$ being the initial (unperturbed) normalized and the final normalized emittance in the plane of interest, respectively, and γ the relativistic Lorentz factor at the undulator. Tanaka’s formula for the gain length can be revised via the following *ansatz* to estimate the 3-D gain length in the presence of collective effects [48]:

$$L_{G,coll} \approx \frac{L_{G,3D}}{1 - \pi \langle \theta_{coll}^2 \rangle / \theta_{th}^2} \tag{15}$$

where $L_{G,3D}$ is the 3-D power gain length as calculated by Xie [53] and $\theta_{th} = \sqrt{\lambda/L_{G,3D}}$. The electron beam slice transverse emittance and the slice energy spread at the undulator are taken into account in $L_{G,3D}$; the information on the projected emittance growth, which is uniquely determined by the initial beam parameters and the linac setting [58], is brought about by $\langle \theta_{coll}^2 \rangle$. The range of application of Equation (15) is $\langle \theta_{coll}^2 \rangle < \theta_{th}^2 / \pi$; this describes the approximate physical picture in which larger values of $\langle \theta_{coll}^2 \rangle$ are expected to inhibit the FEL process. Equation (15) aims to generalize Xie’s formalism, so that $L_{G,coll}$ reduces to $L_{G,3D}$ either for null collective effects $\langle \theta_{coll}^2 \rangle = 0$ or large β_u , for any *pre-set* emittance growth, as shown in Equation (14) and in Figure 7.

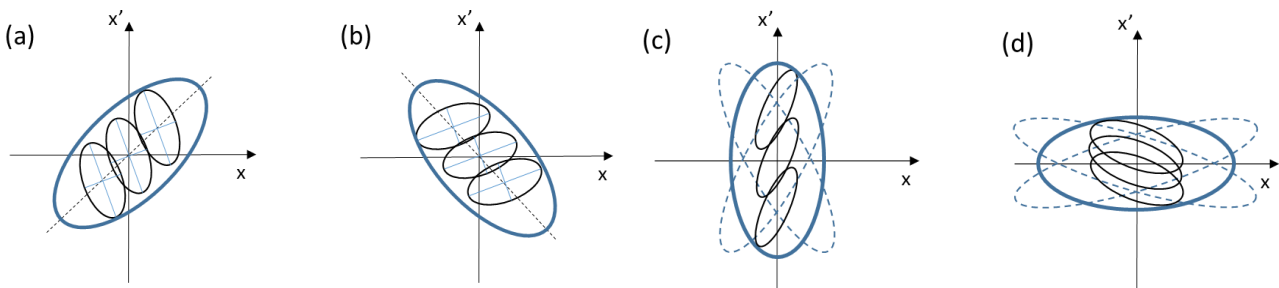


Figure 7. Mechanism of emittance growth in the transverse phase space, due to kicks by collective effects (cartoon). **(a)** Two macro-slices are displaced along the direction of the kick with respect to an unperturbed macro-slice (inner centered ellipse). The projected emittance has grown (outer ellipse). **(b)** Same as in (a), after $\pi/2$ betatron phase advance. The area of the outer ellipse remains constant *after* the kick. **(c)** The beam is matched at the entrance of the undulator to some design Twiss parameters. The optics is smooth in a way that Twiss parameters β and α vary little along the undulator (dashed outer ellipses). Since β_u is small, the macro-slices are largely dispersed within the angular divergence corresponding to $\langle \theta_{coll}^2 \rangle \neq 0$ (solid line ellipse). **(d)** Same as in (c), but with β_u large. The macro-slices largely overlap within angular divergence, *i.e.*, $\langle \theta_{coll}^2 \rangle \rightarrow 0$ (solid line ellipse). Picture published in [48]. Copyright (2014) by The American Physical Society.

It is worth pointing out that Equation (15) aims primarily to identify the dependence of the gain length on the misalignment of bunch slices in the transverse phase space. In this sense, the π term at the denominator should be taken as indicative. The only experimental attempt, to the author’s knowledge, that was carried out to verify such a dependence was reported in [57]. There, a fitting was applied to experimental results and the resultant coefficient showed a deviation from the analytical model, even if the dependence on the projected emittance was confirmed. A discussion on the possible reasons behind the partial agreement of experimental results and the analytical model can be found in [48]. In general, one could imagine that the numerical coefficient at the denominator of Equation (15) depends in turn on the range of electron beam parameters under consideration.

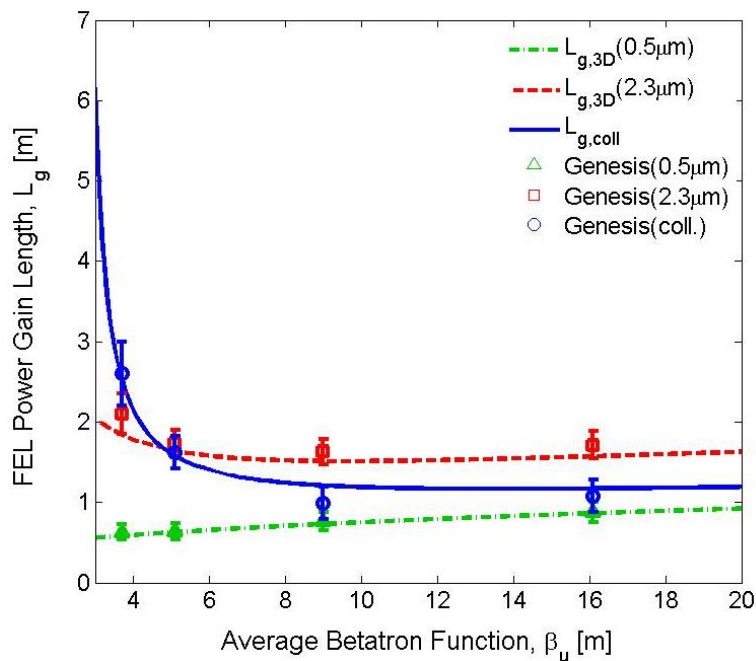


Figure 8. Gain length as function of the average betatron function in the undulator: analytical (lines) and from Genesis simulation results (symbols) (data from Table 1 in [44]). Error bars show the maximum variation of the gain length fit over several simulation runs. For each run used to fit $L_{g, coll}$ (blue circles), several random distributions of the bunch’s macro-slices in the transverse phase space were generated. In this case, each distribution (in each transverse plane) corresponds to a normalized projected emittance of $2.3 \mu\text{m}$, while the slice emittance is $0.5 \mu\text{m}$ for all slices. The projected beam size is forced to fit the average betatron function selected for that run. For the two other cases shown in the Figure, the projected and the slice normalized emittances are equal, with value $0.5 \mu\text{m}$ (green triangles) and $2.3 \mu\text{m}$ (red squares), respectively. The average betatron function used for the abscissa is the geometric mean of the horizontal and the vertical β averaged along the undulator. Picture published in [48]. Copyright (2014) by The American Physical Society.

A quantitative comparison of $L_{G, coll}$ and $L_{G, 3D}$ as function of β_u is shown in Figure 8. The Xie-defined gain length $L_{G, 3D}$ was computed for beam slice normalized emittances of $0.5 \mu\text{m}$ (green dashed-dotted line) and $2.3 \mu\text{m}$ (red dashed line). In these cases the projected emittances coincide with the slice values since all slices are well aligned in phase space. A bunch slice was defined as long as

~3 μm, which is longer than the cooperation length (~1 μm), and sufficiently shorter than the undulator total slippage length (~10 μm). $L_{G, coll}$ was computed for a normalized slice emittance of 0.5 μm but a 2.3 μm normalized *projected* emittance (blue solid line). The larger value of the latter is determined by the misalignment of the bunch slices in the phase space. The analytical predictions are in good agreement with the simulation results obtained with the Genesis code [65]. Most of UV and X-ray FELs tend to have β_u small in order to maximize the transverse overlap of electrons and photons in the undulator. Figure 8 suggests that a beam focusing less tight than foreseen for an ideal beam, might lead to better results for the situation of a highly diluted projected emittance.

The physics depicted so far applies in principle to both SASE and externally seeded, high gain FELs because, independently from the FEL start-up signal, they both rely on the amplification of undulator radiation through the formation of bunching at the resonance wavelength. In practice, however, in a SASE FEL the entire bunch participates to lasing, while for externally seeded FELs generally only the seeded portion of the electron bunch is relevant to lasing. In other words, the present analysis applies only to the lasing (seeded) portion of the electron bunch.

6.3. Optimization Study

We assume that the CSR and the GTW kicks to be uncorrelated, therefore adding in quadrature. According to Equation (14), the final normalized (horizontal) emittance subject to the effects of CSR in n consecutive compression stages and to GTW in m linac sections, is provided by the determinant of the “sigma matrix” computed at the linac end [48]:

$$\varepsilon_{n,f} \cong \varepsilon_{n,0} \sqrt{(1 + P_{CSR}^{BC1})(1 + P_{CSR}^{BC2}) \dots (1 + P_{CSR}^{BCn})(1 + P_{GTW}^{L1})(1 + P_{GTW}^{L2}) \dots (1 + P_{GTW}^{Ln})} \approx \varepsilon_{n,0} \sqrt{1 + \sum_{i=1}^n P_{CSR}^i + \sum_{j=1}^m P_{GTW}^j} \quad (16)$$

The identity of Equation (16) and Equation (14) allows us to compute $\langle \theta_{coll}^2 \rangle$ once β_u and $\varepsilon_{n,f}$ are known. The “kick factors” P_{CSR}^i, P_{GTW}^j depend on the electron beam charge, duration, energy, and Twiss parameters. An expression for the kick factors is given in [48] but a discussion of their analytical derivation is too detailed for this article. Nevertheless, it is worthwhile to stress here that P_{CSR}^i, P_{GTW}^j have *opposite* dependence on the *bunch length*, whereas the former is larger for shorter bunches. This suggests that an optimum value for the bunch duration at the undulator can be found that minimizes the overall impact of CSR and GTW on the projected emittance and thus on $B_{n,f}$. Figure 9 shows the 5-D normalized brightness. The degradation factors introduced in Equation (5) now take into account the impact of CSR and GTW transverse kicks to the bunch slices as the beam travels along the accelerator. The dominant contribution of either CSR or GTW on the projected emittance and final brightness at the undulator depends not only on the electron beam parameters (approximately the same values were adopted in the FERMI [66] and the LCLS linac [67]), but also on the accelerator wakefield and the compression strength. In fact, once the initial bunch charge, duration, and emittance are defined, a larger compression factor will determine a shorter bunch along the downstream accelerator, thereby a weaker effect from GTW but also a larger emittance growth by CSR in the compressor itself. Moreover, similar electron beam parameters and compression strengths do not ensure the same final brightness in accelerators that adopt RF cavities of different internal geometry. The latter is strictly related to the strength of the GTW

that in Figure 9 is shown to dominate the brightness in FERMI (left plot), while it is almost transparent to beam quality in the LCLS case (right plot).

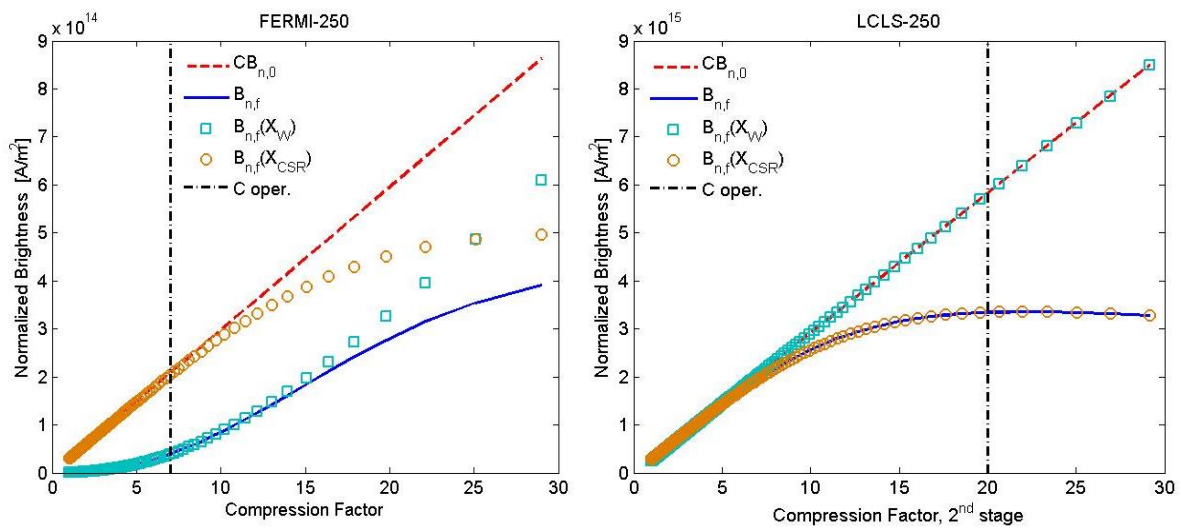


Figure 9. Electron beam z-projected five-dimensional (5-D) brightness, as function of the bunch length compression factor, for a 250 pC beam in the FERMI (left plot) and the LCLS S-band linac (data from [67]). The nominal (unperturbed) brightness is in dashed line, the effective (perturbed) brightness is in solid line, coherent synchrotron radiation (CSR, circles) and geometric transverse wakefield (GTW, squares) dominated brightness is also shown. The dash-dot line identifies the operational compression factor. The two linacs differ in the strength of the GTW, which governs the brightness of the FERMI beam. CSR effects dominate in LCLS, instead, due to much stronger compression. Pictures published in [58]. Copyright (2014) by The American Physical Society.

Figure 10 shows that an optimum can be found for the 6-D brightness as function of the compression factor. Compared to the 5-D brightness in Figure 9, the final uncorrelated energy spread (assumed to be linearly proportional to the compression factor) is now included. $B_{n,f}$ is lowered w.r.t the ideal (invariant) case for the following reasons: at small C , a long bunch excites strong GTW, whilst at large C , CSR in the compressor becomes more important; also, an excess of energy spread is required by the laser heater to damp the microbunching instability. For beam and accelerator parameters similar to those in FERMI, an increase of the 3-D gain length by 15% w.r.t. the definition by M. Xie is predicted, due to degradation of the projected emittance; the slice emittance is assumed to be preserved as at the injector level. More dramatic effects on $L_{G, coll}$ are expected if the compression factor is not properly set in order to balance and partially cancel CSR and GTW kicks.

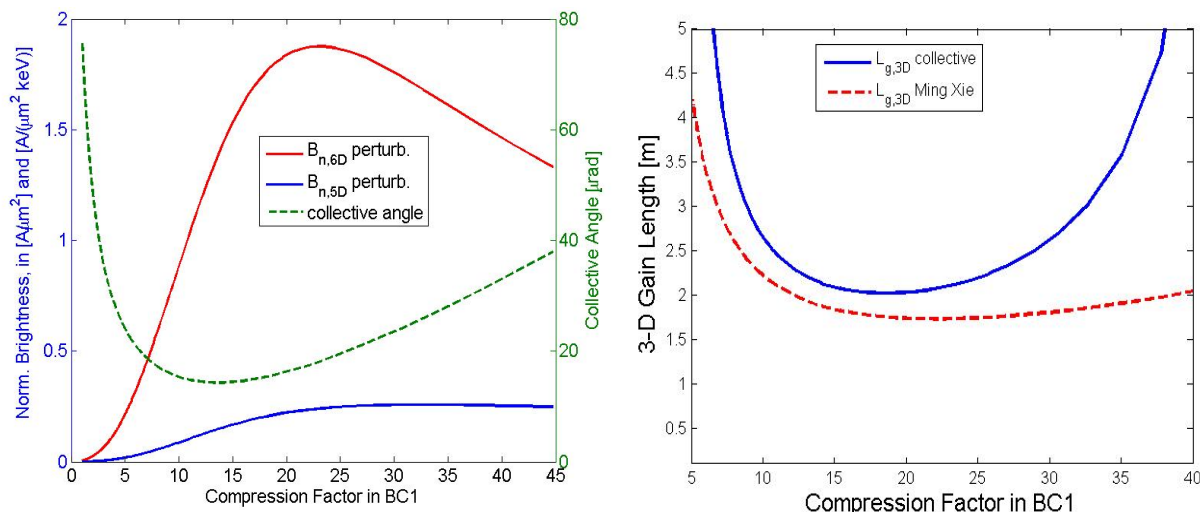


Figure 10. The final 5-D and 6-D normalized brightness and the collective angle are evaluated vs. the compression factor in BC1 (left panel), for a 500 pC bunch charge in the FERMI S-band linac (data from [48]). The 3-D gain length (right) is evaluated in the M. Xie sense and in presence of collective effects, for the same range of compression strengths. Pictures published in [48]. Copyright (2014) by The American Physical Society.

7. Conclusions

Merit functions of high gain SASE FELs have been reviewed for the 1-D; cold electron beam limit. They allow a preliminary estimation of electron beam and undulator parameters. Three different approaches to the design of an FEL linac-driver; depending upon FEL and user requirements; have been discussed. The dependence of the M. Xie-defined 3-D gain length on the electron beam 6-D normalized brightness has been analyzed; permitting a more detailed characterization of the electron bunch slice parameters. The model has further been extended to the inclusion of projected transverse emittances through a re-definition of the 3-D gain length; consistent with the well-known one of M. Xie when the projected beam parameters collapse to the slice values. This extended 3-D model allows the FEL designer to further optimize the design parameters; for example; Twiss parameters in the undulator and electron bunch length compression factor.

In summary, the analysis provided in such a ready-to-use form highlights the need for different approaches to FEL design, primarily depending on the FEL wavelength. When bunch slice parameters are considered, the opposite dependence of the FEL gain length upon radiation diffraction and non-zero transverse emittance effects lead to an optimum value for the undulator average betatron function. An analogous compromise for the value of β_u must be reached when projected emittance growth due to CSR and GTW is also taken into consideration. In this case, the FEL 3-D, z-projected gain length may deviate considerably from the M. Xie value if the compression factor is not properly set.

Acknowledgments

The author is in debt to W. Fawley (Elettra), whose careful reading of this article, and generous sharing of knowledge and experience has made this work possible. The author thanks M. Cornacchia

(Elettra) and P. Craievich (PSI) for a careful reading of this article and their encouragement. This work was funded by the FERMI project of Elettra Sincrotrone Trieste.

Conflict of Interest

The author declares no conflict of interest.

References

1. Madey, J.M.J. Stimulated Emission of Bremsstrahlung in a Periodic Magnetic Field. *J. Appl. Phys.* **1971**, *42*, doi:10.1063/1.1660466.
2. Madey, J.M.J.; Schwetman, M.A.; Fairbank, W.M. A Free Electron Laser. *IEEE Trans. Nucl. Sci.* **1973**, *20*, 980–983.
3. Madey, J.M.J. Wilson Prize article: From vacuum tubes to lasers and back again. *Phys. Rev. Spe. Top. Accel. Beams* **2014**, *17*, 074901.
4. Bonifacio, R.; Casagrande, F.; Cerchioni, G.; De Salvo Souza, L.; Pierini, P.; Piovela, N. Physics of the High-Gain FEL and Superradiance. *La Rivista del Nuovo Cimento* **1990**, *13*, 1–69.
5. Schmöser, P.; Dohlus, M.; Rossbach, J. Ultraviolet and Soft X-Ray Free-Electron Lasers. *Spring. Tract. Mod. Phys.* **2008**, doi:10.1007/978-3-540-79572-8.
6. Saldin, E.L.; Scheidmiller, E.A.; Yurkov, M.V. *The Physics of Free Electron Lasers*; Springer: New York, NY, USA, 2000.
7. McNeil, B.W.J.; Thompson, N.R. X-ray free-electron lasers. *Nat. Photonics* **2012**, *239*, 814–821.
8. Pellegrini, C. The history of free-electron lasers. *Eur. Phys. J. H* **2010**, *37*, 659–708.
9. Huang, Z.; Kim, K.-J. Review of x-ray free-electron laser theory. *Phys. Rev. Spe. Top. Accel. Beams* **2007**, *10*, 034801.
10. Yu, L.H.; Babzien, M.; Ben-Zvi, I.; DiMauro, L.F.; Doyuran, A.; Graves, W.; Johnson, E.; Krinsky, S.; Malone, R.; Pogorelsky, I.; *et al.* High-gain harmonic-generation free-electron laser. *Science* **2000**, *37*, 932–934.
11. Ackermann, W.; Asova, G.; Ayvazyan, V.; Azima, A.; Baboi, N.; Bähr, J.; Balandin, V.; Beutner, B.; Brandt, A.; Brinkmann, R.; *et al.* Operation of a free-electron laser from the extreme ultraviolet to the water window. *Nat. Photon.* **2007**, *1*, 336–342.
12. Emma, P.; Akre, R.; Arthur, J.; Bionta, R.; Bostedt, C.; Bozek, J.; Brachmann, A.; Bucksbaum, P.; Coffee, R.; Decker, F.-J.; *et al.* First lasing and operation of an angstrom-wavelength free-electron laser. *Nat. Photon.* **2010**, *4*, 641–647.
13. Ishikawa, T.; Aoyagi, H.; Asaka, T.; Asano, Y.; Azumi, N.; Bizen, T.; Ego, H.; Fukami, K.; Fukui, T.; Furukawa, Y.; *et al.* A compact X-ray free-electron laser emitting in the sub-angstrom region. *Nat. Photon.* **2012**, *6*, 540–544.
14. Amann, J.; Berg, W.; Blank, V.; Decker, F.-J.; Ding, Y.; Emma, P.; Feng, Y.; Frisch, J.; Fritz, D.; Hastings, J.; *et al.* Demonstration of self-seeding in a hard X-ray free-electron laser. *Nat. Photon.* **2012**, *6*, 693–698.
15. Allaria, E.; Appio, R.; Badano, L.; Barletta, W.A.; Bassanese, S.; Biedron, S.G.; Borga, A.; Busetto, E.; Castronovo, D.; Cinquegrana, P.; *et al.* Highly coherent and stable pulses from the FERMI seeded free-electron laser in the extreme ultraviolet. *Nat. Photon.* **2012**, *6*, 699–704.

16. Allaria, E.; Castronovo, D.; Cinquegrana, P.; Craievich, P.; Dal Forno, M.; Danailov, M.; D'Auria, G.; Demidovich, A.; De Ninno, G.; Di Mitri, S.; *et al.* Two-stage seeded soft-X-ray free-electron laser. *Nat. Photon.* **2013**, *7*, 913–918.
17. Kondratenko, A.M.; Saldin, E.L. Generation of coherent radiation by a relativistic electron beam in an undulator. *Partic. Accel.* **1980**, *10*, 207–216.
18. Sprangle, P.; Tang, C.-M.; Manheimer, W.M. Nonlinear theory of free-electron lasers and efficiency enhancement. *Phys. Rev. A* **1980**, *21*, 302–318.
19. Haus, H. Noise in free-electron laser amplifier. *IEEE J. Quant. Electron.* **1981**, *17*, 1427–1435.
20. Bonifacio, R.; Pellegrini, C.; Narducci, L.M. Collective instabilities and high-gain regime in a free-electron laser. *Opt. Commun.* **1984**, *50*, 373–378.
21. Kroll, N.M.; McMullin, W.A. Stimulated emission from relativistic electron passing through a spatially periodic transverse magnetic field. *Phys. Rev. A* **1978**, doi:10.1103/PhysRevA.17.300.
22. Gover, A.; Livni, Z. Operation Regimes of Cerenkov-Smith-Purcell Free Electron Lasers and T.W. Amplifiers. *Opt. Commun.* **1978**, *26*, 375–380.
23. Shih, C.C.; Yariv, A. Inclusion of space-charge effects with Maxwell's equations in the single-particle analysis of free-electron lasers. *IEEE J. Quant. Electron.* **1981**, *17*, 1387–1394.
24. Dattoli, G.; Marino, A.; Renieri, A.; Romanelli, F. Progress in the Hamiltonian picture of the free-electron laser. *IEEE J. Quant. Electron.* **1981**, *17*, 1371–1387.
25. Pierce, J.R. *Traveling-Wave Tubes*; Van Nostrand Company, Inc.: New York, NY, USA, 1950.
26. Colson, W.B. The nonlinear wave equation for higher harmonics in free-electron laser. *IEEE J. Quant. Electron.* **1981**, *17*, 1417–1427.
27. Bonifacio, R.; McNeil, B.W.; Pierini, P. Superradiance in the high-gain free-electron laser. *Phys. Rev. A* **1989**, *40*, 4467–4475.
28. Murphy, J.; Pellegrini, C.; Bonifacio, R. Collective instability of a free electron laser including space charge and harmonics. *Opt. Commun.* **1985**, *53*, 197–202.
29. Murphy, J.; Pellegrini, C. Generation of High Intensity Coherent Radiation in the Soft X-ray and VUV Region. In Proceedings of the International Conference on Quantum Electronics, San Diego, CA, USA, June 1984.
30. Kim, K.-J. Brightness, coherence and propagation characteristics of synchrotron radiation. *Nucl. Instrum. Meth. Phys. Res. A* **1986**, *246*, 71–76.
31. Leujeune, C.; Aubert, J. *Emission and Brightness: Definitions and Measurements*; Academic Press, Inc.: Paris, France, 1980; pp. 159–259.
32. Barletta, W.A.; Sessler, A.M.; Yu, L.-H. Physically transparent formulation of a free-electron laser in the linear gain regime. *Nucl. Instrum. Meth. Phys. Res. A* **1993**, *331*, 491–495.
33. Yu, L.-H. Generation of intense UV radiation by subharmonically seeded single-pass free-electron lasers. *Phys. Rev. A* **1991**, *44*, 5178–5193.
34. Yu, L.H.; Di Mauro, L.; Doyuran, A.; Graves, W.S.; Johnson, E.D.; Heese, R.; Krinsky, S.; Loos, H.; Murphy, J.B.; Rakowsky, G.; *et al.* First ultraviolet high-gain harmonic-generation free-electron laser. *Phys. Rev. Lett.* **2003**, *91*, 074801.
35. Labat, M.; Bellaveglia, M.; Bougeard, M.; Carré B.; Ciocci, F.; Chiadroni, E.; Cianchi, A.; Couprie, M.E.; Cultrera, L.; Del Franco, M.; *et al.* High-gain harmonic-generation free-electron laser seeded by harmonics generated in gas. *Phys. Rev. Lett.* **2011**, *107*, 224801.

36. Giannessi, L.; Bellaveglia, M.; Chiadroni, E.; Cianchi, A.; Couprie, M.E.; Del Franco, M.; Di Pirro, G.; Ferrario, M.; Gatti, G.; Labat, M.; *et al.* Superradiant cascade in a seeded free-electron laser. *Phys. Rev. Lett.* **2013**, *110*, 044801.
37. Liu, B.; Li, W.B.; Chen, J.H.; Chen, Z.H.; Deng, H.X.; Ding, J.G.; Fan, Y.; Fang, G.P.; Feng, C.; Feng, L.; *et al.* Demonstration of a widely-tunable and fully-coherent high-gain harmonic-generation free-electron laser. *Phys. Rev. Spe. Top. Accel. Beams* **2013**, *16*, 020704.
38. Dowell, D. The Limits of Beam Brightness from Photocathode RF Guns. In Proceedings of the 32th International Free Electron Laser Conference, Malmö, Sweden, 23–27 August 2010.
39. Saldin, E.L.; Schneidmiller, E.A.; Yurkov, M. Longitudinal space charge-driven microbunching instability in the TESLA Test Facility linac. *Nucl. Instr. Meth. Phys. Res. A* **2004**, *528*, 355–359.
40. Huang, Z.; Brachmann, A.; Decker, F.-J.; Ding, Y.; Dowell, D.; Emma, P.; Frisch, J.; Gilevich, S.; Hays, G.; Hering, Ph.; *et al.* Measurements of the linac coherent light source laser heater and its impact on the x-ray free-electron laser performance. *Phys. Rev. Spe. Top. Accel. Beams* **2010**, *13*, 020703.
41. Spampinati, S.; Allaria, E.; Badano, L.; Bassanese, S.; Biedron, S.; Castronovo, D.; Craievich, P.; Danailov, M.B.; Demidovich, A.; De Ninno, G.; *et al.* Laser heater commissioning at an externally seeded free-electron laser. *Phys. Rev. Spe. Top. Accel. Beams* **2014**, *17*, 120705.
42. Hüning, M.; Schlarb, H. Measurement of the beam energy spread in the TTF photo-injector. In Proceedings of the 2003 Particle Accelerator Conference, Portland, OR, USA, 12–16 May 2003.
43. Clarke, J.A. *The Science and Technology of Undulators and Wigglers*; Oxford University Press: Oxford, UK, 2004.
44. Bahrtdt, J.; Ivanyushenkov, Y. Short Period Undulators for Storage Rings and Free Electron Lasers. *J. Phys.* **2013**, *425*, 032001.
45. Shumail, M.; Bowden, G.; Chang, C.; Neilson, J.; Tantawi, S. Beam dynamics studies of a helical X-band RF undulator. *AIP Conf. Proc.* **2012**, *1507*, 752–756.
46. Chang, C.; Liang, J.; Hei, D.; Becker, M.F.; Tang, K.; Feng, Y.; Yakimenko, V.; Pellegrini, C.; Wu, J. High-brightness X-ray free-electron laser with an optical undulator by pulse shaping. *Opt. Express* **2013**, *21*, 32013–32018.
47. Petrillo, V.; Serafini, L.; Tomassini, P. Ultrahigh brightness electron beams by plasma-based injectors for driving all-optical free-electron lasers. *Phys. Rev. Spe. Top. Accel. Beams* **2008**, *11*, 070703.
48. Di Mitri, S.; Spampinati, S. Estimate of free electron laser gain length in the presence of electron beam collective effects. *Phys. Rev. Spe. Top. Accel. Beams* **2014**, *17*, 110702.
49. Di Mitri, S.; Cornacchia, M. Electron beam brightness in linac drivers for free-electron-lasers. *Phys. Rep.* **2014**, *539*, 1–48.
50. Pellegrini, C. Progress towards a Soft X-ray FEL. *Nucl. Instrum. Meth. Phys. Res. A* **1988**, *272*, 364–367.
51. Yu, L.-H.; Krinsky, S.; Gluckstern, R.L. Calculation of universal scaling function for free-electron-laser gain. *Phys. Rev. Lett.* **1990**, *64*, doi:10.1103/PhysRevLett.64.3011.
52. Chin, Y.-H.; Kim, K.-J.; Xie, M. Three-dimensional free electron laser dispersion relation including betatron oscillations. *Nucl. Instrum. Meth. Phys. Res. A* **1992**, *318*, 481–488.

53. Xie, M. Design optimization for an x-ray free electron laser driven by SLAC linac. In Proceedings of the 16th IEEE Particle Accelerator Conference, Dallas, TX, USA, 1–5 May 1995; pp. 183–185.
54. Saldin, E.L.; Schneidmiller, E.A.; Yurkov, M.V. Design Formulas for VUV and X-Ray FELs. In Proceedings of the 26th International Free Electron Laser Conference, Trieste, Italy, 3 September 2004.
55. Saldin, E.L.; Schneidmiller, E.A.; Yurkov, M.V. The general solution of the eigenvalue problem for a high-gain FEL. *Nucl. Instrum. Meth. Phys. Res. A* **2001**, *475*, 86–91.
56. Tanaka, T.; Kitamura, H.; Shintake, T. Consideration on the BPM alignment tolerance in X-ray FELs. *Nucl. Instrum. Meth. Phys. Res. A* **2004**, *528*, 172–178.
57. Chae, Y.-V.; Lumpkin, A.H.; Erdmann, M.; Lewellen, J.W.; Milton, S.V. An Experimental Study of the Beam-Steering Effect on the FEL Gain at LEUTL’s Segmented Undulators. In Proceedings of the 11th International Free Electron Laser Conference, Trieste, Italy, 3 September 2004.
58. Di Mitri, S. Maximum brightness of linac-driven electron beams in the presence of collective effects. *Phys. Rev. Spe. Top. Accel. Beams* **2011**, *16*, 050701.
59. Guetg, M.W.; Beutner, B.; Prat, E.; Reiche, S. Optimization of free electron laser performance by dispersion-based beam-tilt correction. *Phys. Rev. Spe. Top. Accel. Beams* **2015**, *18*, 030701.
60. Freund, H.P.; O’Shea, P.G. The effect of a matched electron beam on high-gain free-electron-laser amplifier performance. *Phys. Rev. Lett.* **1998**, *80*, doi:10.1103/PhysRevLett.80.520.
61. Reiche, S. Compensation of FEL gain reduction by emittance effects in a strong focusing lattice. *Nucl. Instr. Meth. Phys. Res. A* **2000**, *445*, 90–94.
62. Geloni, G.; Kocharyan, V.; Saldin, E.L. The effects of betatron motion on the preservation of FEL microbunching. DESY 11–081, 2011. Available online: <http://arxiv.org/abs/1105.3878v1> (accessed on 19 May 2011).
63. Minty, M.G.; Zimmermann, F. *Beam Techniques—Beam Control and Manipulation*; Report No. SLAC-R-621; SLAC: Stanford, CA, USA, 2003.
64. Chao, A.W.; Tigner, M. *Handbook of Accelerator Physics and Engineering*, 3rd ed.; World Scientific: Singapore, 2006.
65. Reiche, S.; Goldammer, K.; Musumeci, P. Recent Upgrade to the Free-electron Laser Code Genesis 1.3. In Proceedings of the 22nd Particle Accelerator Conference, Albuquerque, NM, USA, 25–29 June 2007.
66. Di Mitri, S.; Allaria, E.; Appio, R.; Badano, L.; De Ninno, G.; Castronovo, D.; Cornacchia, M.; Craievich, P.; Ferry, S.; Frolich, L.; *et al.* Recent Commissioning Experience on the FERMI@Elettra First Bunch Compressor Area: Investigations of Beam Dynamics, Modeling and Control Software. In Proceedings of the 32nd International Free Electron Laser Conference, Malmö, Sweden, 23–27 August 2010.
67. Ding, Y.; Brachmann, A.; Decker, F.-J.; Dowell, D.; Emma, P.; Frisch, J.; Gilevich, S.; Hays, G.; Hering, Ph.; Huang, Z.; *et al.* Measurements and Simulations of Ultralow Emittance and Ultrashort Electron Beams in the Linac Coherent Light Source. *Phys. Rev. Lett.* **2009**, *102*, 254801.